Wind Energy and the Turbulent Nature of the Atmospheric Boundary Layer

Matthias Wächter, Hendrik Heißelmann, Michael Hölling, Allan Morales, Patrick Milan, Tanja Mücke, Joachim Peinke, Nico Reinke, Philip Rinn*

This paper has been submitted to the Journal of Turbulence on February 8, 2012.

Abstract

The challenge of developing a sustainable and renewable energy supply within the next decades requires collaborative efforts as well as new concepts in the fields of science and engineering. Here we give an overview on the impact of small-scale properties of atmospheric turbulence on the wind energy conversion process. Special emphasis is given to the noisy and intermittent structure of turbulence and its outcome for wind energy conversion and utilization. Experimental, theoretical, analytical, and numerical concepts and methods are presented. In particular we report on new aspects resulting from the combination of basic research, especially in the field of turbulence and complex stochastic systems, with engineering applications.

${f 1}$ Introduction

Wind Energy is one of of the most promising renewable energies of the presence, see e.g. Ref. [1]. It is therefore of primary importance for future sustainable energy supply systems. During the past decades, considerable advances in science and engineering have lead to wind energy converters (WECs) reaching efficiencies and sizes which appeared impossible only a few years ago.

In contrast to the amazing progress in design and manufacturing of WECs, the understanding of the physics of the energy resource, i.e. the turbulent atmospheric boundary layer, and its interaction with the WECs leaves many open questions and remains insufficient. To give one example, in the context of wind energy commonly Gaussian statistics of fluctuations of wind fields are assumed, which is also reflected in the current industry standard IEC 61400 It is well-known that in turbulence highly intermittent (i.e. non-Gaussian) statistics are found, especially for probability density functions (PDFs) of velocity increments $\delta u_{\tau}(t) = u(t+\tau) - u(t)$. This effect is even stronger in atmospheric flows [3, 4, 5, 6, 7, 8, 9, 10]. Figure 1 shows that for a 7σ event of δu_{τ} the Gaussian PDF underestimates the probability by a factor of 10⁷, compared to the measured statistics. This means if the Gaussian statistics predicts the event to occur every 1250 years, in reality it is expected to happen once every hour. For WECs these increments are directly connected to changes in loads and power output,

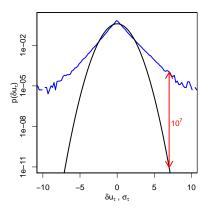


Figure 1: PDF of measured wind speed increments $\delta u_{\tau}(t) = u(t+\tau) - u(t)$ for time lag $\tau = 3s$ (blue line) compared to a Gaussian PDF with same standard deviation (black line). At 7σ both differ by a factor of 10^7 . Note the logarithmic scale of the vertical axis. For details of the measurement please see Ref. [12].

as well as damage statistics [11]. Thus improvements in the understanding of the turbulent nature of the energy resource wind has the potential to improve the efficiency of WECs.

Combining approaches, methods, and results from basic turbulence research, meteorology, stochastics, and measurement technology, improvements in this field can be activated. In this paper we present recent results connected to the mentioned unique statistical properties of atmospheric wind and their effect on wind energy conversion systems. Section 2 is concerned with the typical small-scale intermittency of atmospheric wind fields. Methods for the proper analysis and characterization, as well as the proper experimental reproduction of turbulent flow conditions in a wind tunnel setup, and the impact on WECs are presented in respective subsections. In Sec. 3 we show that stochastic methods are adequate tools to characterize and model the dynamics of power conversion by WECs as a result of interaction between machines and atmospheric turbulence. Section 4 finally gives an outlook to future work.

2 Small-Scale Intermittency

2.1 Analysis and Characterization

Atmospheric wind fields are complex structures, fluctuating in time as well as in space. The industry standard IEC 61400 [2] defines quantities and procedures for considering the in-

^{*}ForWind Center for Wind Energy Research; Turbulence, Wind Energy & Stochastics group TWiSt, Institute of Physics, Carl von Ossietzky University, 26111 Oldenburg, Germany

fluence of atmospheric turbulence on WECs. As a practical approach to wind field characterisation, the ten minute mean value of the horizontal wind speed, $\bar{u} = \langle u(t) \rangle_{10\,min}$, is used together with the standard deviation σ with respect to the same time interval. These quantities are one-point statistics and thus can not reflect the succession of velocity values. Moreover, the dynamics of current WECs is not grasped by ten-minute statistics. Fast load changes on the rotor, the dynamical respons of the WEC, and resulting power output dynamics rather take place at a time scale of the order of 1s.

The IEC standard proposes for a more detailed characterization of wind fields universal power spectral densities of the horizontal wind speed. These are also commonly used for the synthetic generation of wind inflow data [13]. An important limitation of these spectral models are the purely Gaussian statistics of the resulting wind fields, especially in the wind speed increments, which does not reflect experimental results, as shown in Fig. 1.

While necessity and usefulness of standards are beyond doubt, in the recent years growing demand for a more comprehensive and more detailed characterization has become evident. To characterize variations of u in a general way we consider wind speed increments

$$\delta u_{\tau}(t) = u(t+\tau) - u(t) \tag{1}$$

as already introduced in Sec. 1. The moments $\langle (\delta u_{\tau})^k \rangle$ of these increments and their dependence on the scale τ are also called *structure functions* and reflect the variation statistics of order k. It is straightforward to see that the second-order structure function $\langle (\delta u_{\tau})^2 \rangle$ is directly related to the auto-correlation function and thus also to the power spectral density. As $\langle (\delta u_{\tau})^2 \rangle$ grasps only the width of the PDF $p(\delta u_{\tau})$ it becomes clear that, taking only the power spectra into account, Gaussian statistics of $p(\delta u_{\tau})$ are implied. Alternatively to the moments, also the τ -dependence of the PDFs $p(\delta u_{\tau})$ can be investigated, which consequently reflect the variation statistics of all orders.

For practical applications, the high complexity of atmospheric flows has to be further disentangled and a set of crucial parameters and methods has to be defined. A number of advances could already be achieved in this direction. In [4, 5] a model for atmospheric wind speed increment PDFs was presented, reproducing characteristic properties of different locations, such as offshore sites or onshore sites in different terrain. Based on earlier work of Castaing[14] the PDFs are considered as multiple superpositions of Gaussian distributions, combining the intermittency at a given mean wind speed and the typical Weibull distribution of 10 min mean wind speeds. An application example for an offshore site located in the Baltic Sea is presented in Fig. 2. Especially the intermittency and the evolution of the shape of the PDFs with the scale τ is well reproduced by the model. Nevertheless, slight deviations remain. For details, including the derivation of the parameters, please refer to Ref. [5]. This work is currently continued using new findings from extended data analysis of other offshore measurement campaings. In a further step, this concept was embedded into a hierarchical framework for the statistical characterization

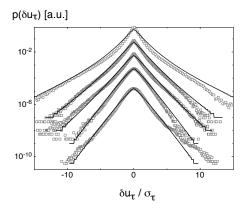


Figure 2: Modeling of atmospheric probability density functions for an offshore site, reproduced after [5]. Symbols represent the normalized PDFs of atmospheric data sets in semi-logarithmic presentation. Solid lines correspond to a model according to Eq. (20) of [5]. All graphs are vertically shifted against each other for clarity of presentation. From top to bottom τ takes the values of (0.2, 10, 20, 200, 2000) s.

of atmospheric turbulence in Ref. [15]. An advanced procedure was proposed for the disentangling of atmospheric wind measurements into subsets which behave similar to homogeneous, isotropic turbulence. It could be shown that for the mentioned subsets the dependence of the intermittency parameter λ^2 (for a definition please refer to [15]) on the time scale τ corresponds with Kolmogorov's refined scaling law for homogeneous isotropic turbulence of 1962 [16],

$$\langle (\delta u_{\tau})^n \rangle \propto \tau^{\frac{n}{3} - \mu \frac{n(n-3)}{18}}$$
 (2)

Here, μ characterizes the evolution of intermittency in the scaling behavior of structure functions. The dependence $\lambda^2(\tau) = \lambda_0^2 - \frac{1}{9}\mu\log\tau$ is covered by Eq. (2) for n=4, see appendix of [15]. For different atmospheric data sets the value of $\mu=0.26\pm0.4$ reported in the literature [16] could be confirmed.

In this section we present a similar model for PDFs of atmospheric wind speed fluctuations $u'(t) = u(t) - \bar{u}$ with $\bar{u} = \langle u(t) \rangle_{10 \,\mathrm{min}}$, which is a common quantity in the wind energy field. As u' constitutes one-point statistics it should nevertheless be clearly distinguished from the two-point statistics of increments δu_{τ} . A first approach based on cup anemometer data was included in [15]. In our extended analysis here we use one month of ultrasonic data measured at the offshore research platform FINO I, where the wind speed u is taken in the direction of \bar{u} . Ultrasonic anemometers offer higher quality data in terms of higher sampling rates (10 Hz in our case) than cup anemometers and avoid effects of rotational inertia. In contrast to laboratory turbulence, the pdf p(u') is strongly intermittent, see figure 3(a). Even after conditioning the statistics of u' on a certain value of \bar{u} the intermittency persists, see $p(u'|\bar{u})$ in figure 3(b). Thus, the source of intermittency is not only the non-stationarity of the mean wind speed. As shown in [15] in fact the statistics of u' seem to follow a Gaussian distribution within single 10minute time spans. Therefore, the effect of the atmosphere can be understood as mixing these clean Gaussian statistics

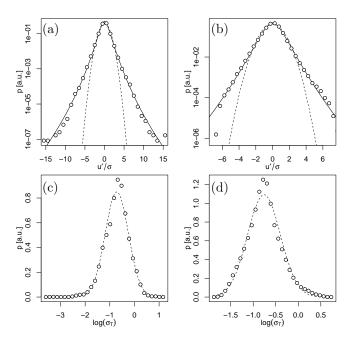


Figure 3: Statistics of fluctuations u' of atmospheric wind speeds, measured at the German offshore research platfrom FINO I. Parts (a) and (b) present empirical PDFs of fluctuations u' (symbols), model results according to Eq. Eq. (3) (solid lines) and Gaussian PDFs for comparison (dashed lines). Part (a) shows p(u') for all data and (b) $p(u'|\bar{u})$ conditioned on $\bar{u} = (10 \pm 1) \, \text{m/s}$. In parts (c) and (d) we show distributions of logarithms of the standard deviations σ_T . Part (c) again represents $p(\log \sigma_T)$ for the full data set while (d) shows $p(\log \sigma_T|\bar{u})$ conditioned as in (b).

by the randomization of the ten-minute standard deviations σ_T over periods longer than 10 minutes. The distribution $p(\sigma_T)$ can in most cases at least approximately be described by a log-normal distribution [17], compare Figs. 3(c) and (d).

Inspired by the works of Castaing [14] and Boettcher [5] we can now set up an improved model the PDFs of u' as superpositions of Gaussian distributions with different standard deviations, where the PDF of these standard deviations itself is log-normal:

$$p(u') = \int_0^\infty \frac{d\sigma_T}{\sigma_T^2} \frac{1}{2\pi\alpha} \underbrace{\exp\left\{-\frac{u'^2}{2\sigma_T}\right\}}_{\text{Gaussian}} \underbrace{\exp\left\{-\frac{(\log\frac{\sigma_T}{\sigma_m})^2}{2\alpha^2}\right\}}_{\text{log-normal PDF}},$$
for single σ_T of σ_T values
$$(3)$$

where $\sigma_m = \exp{\{\langle \log \sigma_T \rangle\}}$ and $\alpha^2 = \langle (\log \sigma_T)^2 \rangle - \langle \log \sigma_T \rangle^2$. In this model, α^2 plays a similar role as λ^2 in the statistics of increments, and quantifies the amount of intermittency in the PDF. This compact model reproduces the empirical values quite well, as presented in figures 3(a) and (b) for the unconditioned and conditioned PDFs of atmospheric wind speed fluctuations, respectively. The quality of results for our example is even slightly better than in Fig. 2. As all parameters of Eq. (3) can be derived from the basic 10-minute statistics which are commonly measured during field

campaigns for wind energy applications, our model gives access to the high-frequency statistics of u' even if no high-frequency data have been recorded. Together with the results for increments shown in Fig. 2, now models of both the one-point and two-point statistics for wind data exist. Their validity was shown using examples of offshore data. Using these models, complete and straightforward characterizations of both the wind speed u and wind speed increments u_{τ} are possible. Besides the models described here, there are other possibilities, such as special parametric distributions, but a systematic comparison is beyond the scope of this paper. We believe that a strength of our approach is its motivation by the physics of turbulence and in the easy access to the necessary parameters.

A proper characterization forms the basis for an improved understanding of atmospheric turbulence, which in term leads to improved experiments, models, synthetic wind fields, and load estimations, to name a few examples.

2.2 Experimental Reproduction

Besides an improved characterization and description of atmospheric wind fields, it is of special relevance for experimental investigations to properly reproduce these statistical features in the wind tunnel. This includes in particular a rescaling of spatial correlations (e.g., gusts) to dimensions of the wind tunnel and the models in use, respectively. Up to today there exists no method for the generation of turbulence that allows for a complete control of spatial correlations nor statistical properties of the resulting flow on all scales due to the natural decay of laboratory turbulence. This subsection describes current results concerning options and limits of artificially created turbulence by an active grid with respect to spatial structures and reproducibility.

Active grid

To overcome the problem of fixed solidity and fixed effective mesh size of classical grids for the generation of turbulence, a more flexible and powerful set-up was built up at the University of Oldenburg. The so-called active grid, cf. [18, 19], allows for the generation of turbulent flows by actively rotating nine vertical and seven horizontal axes with squareshaped vanes mounted to them (see Fig. 4). Each of these axes is controlled by a stepper motor and can be accessed individually with a maximum resolution of 51200 steps per rotation. This grid can be used in passive mode with statically adjusted axes, as well as in active mode with moving axes. In active mode each axis can be driven by e.g. sinusoidal or randomized signal resulting in a time-dependent solidity. This allows for a flexible excitation of the flow. Figure 5 shows a comparison of the PDFs for different time lags measured in passive mode with all vanes oriented parallel to the inflow direction resulting in the minimum achievable solidity (a) and the PDFs measured in active mode with a randomized signal (b). It can clearly be seen that in the static configuration only for the smallest time scales intermittency is observed. For the active mode, on the other hand, a pronounced intermittency is generated for a wider

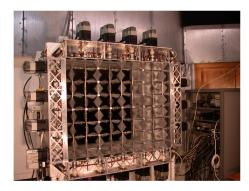


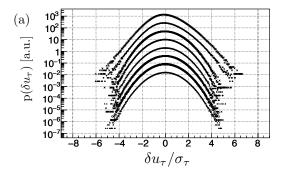
Figure 4: Active grid mounted to the wind tunnel outlet at the University of Oldenburg. Visible are the horizontal and vertical axes with mounted vanes and individual stepper motors.

range of time scales, as it was also implemented in the excitation signal [20]. The direct coupling of the motion of the individual axes to the resulting characteristics of the generated flow field therefore allows for a defined manipulation of the flow.

Reproducibility

To investigate the reproducibility of turbulent wind fields with different spatial structures created by the active grid, a control signal for the axes as shown in Fig. 6(a) was realized. The complete protocol consists of several of these sequences in which the angular position of the axis changes from 90° to 72° , 54° , 36° , 18° and 0° . In the setup 90° corresponds to a vertical orientation of the mounted vanes with respect to the incoming wind velocity. The time between each change in the angular position was 0.2 seconds. In order to keep the overall solidity of the grid constant for the whole sequence the protocol for the outer eight axes has been programmed with an offset of 90°. For the characterization of the resulting flow, velocity measurements on the centerline behind the grid have been carried out using hot-wire anemometry with a sampling frequency of 40 kHz for different distances d to the grid varying from $10\,\mathrm{cm}$ to 180 cm with $\Delta d = 10$ cm and an inflow velocity of 16 m/s. Figure 6(b) shows the resulting velocity of the implemented sequence with increasing distance to the grid. It can clearly be seen that the different angles of the axes result in pulses with increasing velocities. It can also be seen that the measured flow velocities change with increasing distance to the active grid, which indicates a decay of the generated velocity pulses and spatial structures, respectively.

To investigate the decaying process of these structures in more detail, three excitation protocols with several identical sequences like presented in Fig. 6(a) have been realized where just the length of the pulses has been changed. Sequences with pulses of 0.2, 0.5, and 1 second duration have been implemented and used for the excitation of the grid's axes. In order to determine where the uncorrelated decay of natural turbulence starts to dominate, each excitation sequence has been identified in the measured velocity time series and separated. To filter out spatial structures from the



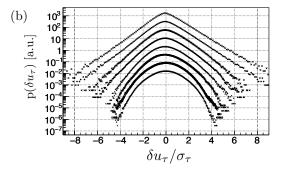


Figure 5: (a) PDFs of velocity increments $\delta u = u(t+\tau) - u(t)$ for passive mode of the active grid. Time lags τ from top to bottom are $2.5 \cdot 10^{-4} \, \mathrm{s}$, $5 \cdot 10^{-4} \, \mathrm{s}$, $2.5 \cdot 10^{-3} \, \mathrm{s}$, ..., $5 \cdot 10^{-1} \, \mathrm{s}$. (b) PDFs of velocity increments for the active grid with stochastic control of vane movement. Time lags τ are as in (a). The graphs are shifted vertically for clarity of presentation.

flow, each of these velocity sequences has been high-pass filtered with different filter frequencies starting from $0.14\,\mathrm{Hz}$ up to $133\,\mathrm{Hz}$. Figure 7(a) shows an example of measured velocities for one excitation sequence with a pulse length of 0.2 seconds at distance $d=40\,\mathrm{cm}$ together with the high-pass filtered signal for filter frequencies of $5\,\mathrm{Hz}$ (green) and $40\,\mathrm{Hz}$ (red). The signals are shifted vertically for clarity of presentation. It can clearly be seen that higher filter frequencies result in damping of the impressed pulses.

Furthermore, correlation coefficients have been determined for different realizations of measured velocities using identical filter frequencies. Figure 7(b) shows the average of the resulting correlation coefficients for sequences of all three pulse durations plotted over the filter frequency of the applied high-pass filter. The velocity sequences have been measured at a distance of $d=40\,\mathrm{cm}$ to the grid. The dashed lines represent the corresponding standard deviation for each graph. It can clearly be seen that the filter frequency at which the correlation coefficient drops off increases with shorter pulse durations. Applying Taylor's Hypothesis, this is also in agreement with the equivalent in spatial terms, where shorter excitation pulses correspond to smaller spatial structures and therefore need higher filter frequencies to be filtered out.

To investigate the stability of the generated spatial structures with increasing distance to the grid, the measured ve-

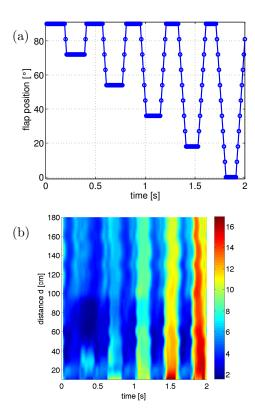


Figure 6: (a) Sequence of realized protocol for the creation of increasing velocity pulses. Each pulse has a duration of 0.2 seconds. (b) Resulting velocity of the implemented sequence with increasing distance to the grid.

locity sequences have been split into isolated single pulses. Conditioned on pulses with identical motion of the vanes, this procedure allows for a similar analysis as already applied to the whole sequence. Based on the split sequences a plot according to Fig. 7(b) can be calculated for each distance d to the grid, conditioned on pulses 1, 2, 3, 4, and 5, respectively, for all three pulse durations. The filter frequency for which the correlation coefficient drops off to 90% of its respective maximum was defined to be the cutoff frequency. It defines the smallest time, and thus the smallest spatial structure, of the generated flow that is not dominated by natural decay and therefore can reproducibly be generated by the active grid. The plots in figure 8 show the cutoff frequency over the distance d to the grid for (a) conditioned on the pulse with the largest resulting velocity difference and (b) conditioned on the pulse with the second largest velocity difference for all pulse durations. The results show that the cutoff frequency for the pulse with the largest velocity difference is nearly constant over the whole distance and the standard deviation for the shortest pulse duration increases with distance (Fig. 8(a)). In Fig. 8(b) a sudden decrease in the cutoff frequency is visible at a distance $d = 130 \,\mathrm{cm}$ for the pulse with the shortest duration of $0.2\,\mathrm{s}$, whereas the cutoff frequencies for the pulses with longer pulse duration stay constant. This indicates, that the spatial structure created by the 0.2 second pulse is not stable over the whole measurement distance, which has to

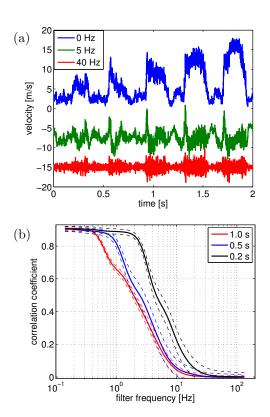


Figure 7: (a) Velocity sequence with pulse duration of 0.2 seconds measured at distance $d=40\,\mathrm{cm}$ to the grid (blue). The green and red curves represent the high-pass filtered signal at filter frequencies of 5 Hz and 40 Hz, respectively. Graphs are shifted vertically for clarity of presentation. (b) Averaged correlation coefficient over cutoff frequency of high-pass filter for excitation sequences with pulse duration of 0.2 s (black), 0.5 s (blue) and 1 s (red). The dashed lines indicate the corresponding standard deviation.

be accounted for in the design of excitation protocols.

Test of standard anemometers

The ability of the active grid to generate turbulent flow situations with reproducible temporal and spatial features, as shown in the previous subsection, provides a powerful tool not only for basic turbulence investigations, but also for the characterization of airfoils and model wind turbines exposed to intermittent wind fields. As an application example, comparative measurements of the same flow situation have been carried out with two standard anemometers for wind energy applications: a *Thies First Class Advanced* cup anemometer and a *Gill Windmaster Pro* 3D ultrasonic anemometer. The signal recorded with a standard 1D hot-wire probe served as a reference, since the hot-wire provides the highest spatial and temporal resolution.

While 1D hot-wire and cup anemometer lack any directional information, the data from the 3D ultrasonic anemometer includes the horizontal wind speed magnitude and direction. However, the alignment of transducers and supporting structures of the sonic anemometer can cause flow disturbances under certain orientations [21]. The used

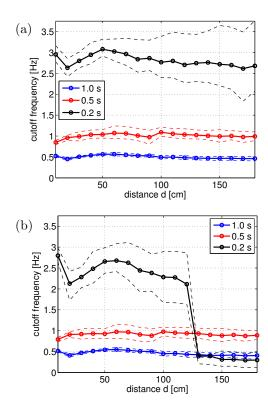


Figure 8: Cutoff frequency over distance d to the grid. The cutoff frequency describes the filter frequency of the applied high-pass filter, where the averaged correlation coefficient of sequences conditioned on (a) the pulse with the highest velocity difference and (b) the pulse with the second highest velocity difference decreased to 90% of its respective maximum. The curves belong to pulses with duration of 0.2s (black), 0.5s (blue) and 1s (red). The dashed lines indicate the corresponding error.

Gill Windmaster Pro an emometer features three support rods with an angular distance of $120^{\circ},$ where the position of the sensor's north spar coincides with the position of one supporting rod. Thus, the northward orientation (0°) of the an emometer implies a support structure being upstream the measurement volume, while a southward (180°) orientation implies free inflow to the measurement volume.

All sensors were calibrated before the measurement and have been successively placed at a distance $d=130\,\mathrm{cm}$ downstream of the active grid with the center of their respective measurement volumes on the centerline of the wind tunnel test section. The excitation protocol of the active grid was chosen in such a way, that the resulting modulated wind flow obeys non-Gaussian statistics as they can be found in atmospheric wind fields.

For each mean wind speed, 30 minutes of data were recorded with hot-wire, cup anemometer and ultrasonic anemometer in northward and southward orientation. The hot-wire data was sampled at 20 kHz and smoothened using an average over 20 samples. The lower-resolving cup anemometer and sonic anemometer were sampled at 4 Hz and 32 Hz, respectively. Figure 9(a) shows a 30 second excerpt of the time series recorded with hot-wire (black), ul-

trasonic anemometer (red) in southward orientation and cup anemometer (blue). A good agreement of the time series for the hot-wire and the sonic anemometer is observed and the fact that all anemometers capture the strong fluctuations at e.g. $t=2{\rm s}$ or $t=13.5{\rm s}$ gives evidence about the robustness and reproducibility of the used excitation protocol. However, the cup anemometer can only resolve the slower and more pronounced gust events. The faster fluctuations of the wind speed (e.g. $t=22{\rm s}$ to $t=25{\rm s}$) cannot be resolved, which on the one hand is due to its low temporal resolution and on the other hand is a result of the spatial extent of the anemometer itself.

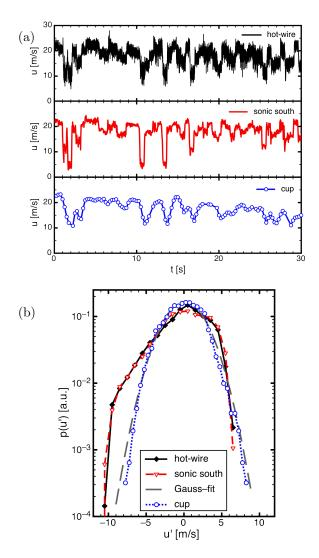


Figure 9: (a) 30-seconds-excerpt of the wind speed data measured with 1D hot-wire anemometer (black), 3D ultrasonic anemometer (red) in southward orientation and cup anemometer (blue). The general evolution of the turbulent flow is covered by all anemometers, but the cup anemometer cannot resolve the fast fluctuations with small amplitudes. (b) PDF of the wind speed fluctuations u' for the down-sampled (4 Hz) time series from (a) with Gaussian fit (dashed gray).

A comparison of the basic statistical quantities commonly used in wind energy, i.e. mean wind speed \bar{u} , standard devi-

ation σ_u and turbulence intensity $TI = \bar{u}/\sigma_u$, for the time series shown in Fig. 9(a) is given in Tab. 1. Only a slight deviation from the hot-wire reference is observed for the ultrasonic anemometer's data, while all quantities of the cup anemometer are significantly lower than the reference. A closer look at the statistics for all sensors is provided in the PDFs of the measured wind speed fluctuations u' in Fig. 9(b). The higher resolved hot-wire data and ultrasonic anemometer data have been down-sampled to the resolution of the cup anemometer at 4 Hz, in order to allow for a comparison of the PDFs. Even the down-sampled hot-wire reference (black) shows a clearly non-Gaussian PDF with higher probabilities for strong wind speed decreases, which is also observed in the PDF of the ultrasonic anemometer (red). In contrast, the PDF of the fluctuations covered by the cup anemometer (blue) obeys a Gaussian distribution as fitted in the plot (dashed gray).

Table 1: Measured mean wind speed \bar{u} , standard deviation σ_u and turbulence intensity TI for the time series from Fig. 9(a).

sensor	\bar{u}	σ_u	TI
hot-wire	17.1 m/s	$3.8\mathrm{m/s}$	22%
sonic south	$17.6\mathrm{m/s}$	$3.5\mathrm{m/s}$	20%
cup	$15.5\mathrm{m/s}$	2.3 m/s	15%

Besides the comparison of the wind speed measurements, it is also worth comparing the wind directions measured with the 3D ultrasonic anemometer in different orientations. For this purpose the PDFs of the wind direction fluctuations $\phi'(t) = \phi(t) - \langle \phi(t) \rangle$ are shown in Fig. 10 for an inflow velocity of about $10 \,\mathrm{m/s}$ (a) and about $20 \,\mathrm{m/s}$ (b). The comparison of the two different orientations for both wind speeds gives evidence of the increased probability for the occurrence of larger direction fluctuations for the northward alignment (0°) of the anemometer. This result is expected, since a supporting rod is located upstream the measuring volume and thus vortex shedding causes wake effects. The self-induced effect is more pronounced for the higher velocity in Fig. 10(b). Additionally, the measured mean wind speed of 16.2 m/s for northward alignment is reduced by approximately 1.4 m/s compared to the southward orientation. Considering the geometry of the ultrasonic anemometer an increasing systematic error in the measurements can be concluded for inflow from 0°, 120° and 240°, respectively.

To conclude this subsection, the active grid offers the generation of turbulent flows with similarly intermittent statistics to atmospheric wind as was shown in [20]. Especially promising in this context is also the generation of reproducible flow structures in a deterministic sense, as it has been shown in this subsection. Besides an emometer testing and characterization, also the interaction of typical structures like airfoils or model wind turbines with reproducible flow fields shall be investigated in the future. It should be noted that the active grid offers also further applications for wind energy research, e.g., generating shear flows [22] or special structures like low level jets [23].

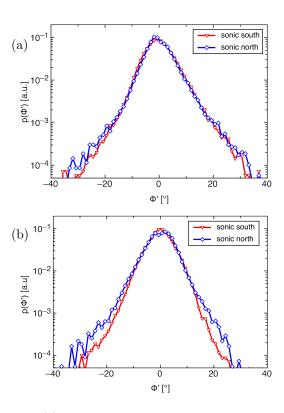


Figure 10: (a) PDF of the wind direction fluctuations measured with the 3D ultrasonic anemometer in northward (blue) and southward (red) orientation at about $10\,\mathrm{m/s}$ inflow velocity. (b) PDF of the wind direction fluctuations measured with the 3D ultrasonic anemometer in northward (blue) and southward (red) orientation at about $20\,\mathrm{m/s}$ inflow velocity.

2.3 Impact on loads and power generation of wind energy converters

The turbulent nature of the wind with its characteristic intermittency can be expected to have a major impact on wind energy converters. These machines operate in the turbulent atmospheric boundary layer and are thus permanently exposed to turbulent wind fields.

To investigate the influence of the turbulent inflow characteristics especially on the loads acting on WECs, numerical studies have been performed. As a numerical turbine model the FAST code by NREL [25] was used together with the WindPACT 1.5 MW virtual turbine [26]. The unique wind field measurement of the German GROWIAN campaign [27, 24] was used as inflow condition. Additionally the Kaimal model of the TurbSim software [28] and a newly developed model based on stochastic processes [29, 30] were used for comparison. In a first analysis, the statistics of rotor torque increments were derived and compared [31]. It was found that the typical intermittency of the wind transfers to a similar intermittency in the rotor torque when the measured wind field is used as input, see Fig. 12(a). The Gaussian increment statistics of the Kaimal wind field, on the other hand, lead to Gaussian torque statistics, supporting the statements above on the implicit Gaussian assumptions in the IEC standard [2]. The intermittent synthetic

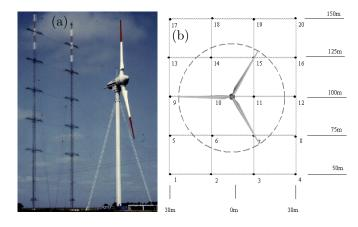


Figure 11: (a) GROWIAN test site of the 1980's [24] and (b) layout of the wind measurement setup, compared to the position of the rotor.

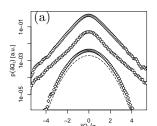
wind field results in much more realistic torque statistics.

Here we present additional results of the rotor thrust forces from the identical numerical setup as above. In Fig. 12(b) thrust increments obtained under the same inflow conditions as in part (a) are compared at $\tau=1\,\mathrm{s}$. We find that the measured wind field leads to a highly intermittent torque PDF, which is well reproduced by the stochastic wind field model. The Kaimal wind field leads to purely Gaussian thrust increment PDFs and thus underestimates extreme thrust loads.

Both torque and thrust form a complete decomposition of forces at the nacelle of a WEC. With these results we can therefore conclude that intermittency is a general property of the wind-generated forces at the WEC. Moreover, thrust forces appear at all types of buildings and structures which are exposed to the wind. This emphasizes again the relevance of our results.

As we observe intermittent statistics of the rotor forces at WECs, it can be expected that the generated electrical power signal is also influenced by this property. In Ref. [32] it could be demonstrated that actually the electrical power signal possesses similarly intermittent dynamics as the wind. These results are confirmed and extended in this paper, see Sec. 3.

From our results we see that the use of Gaussian wind fields in WEC simulation and design must lead to a dramatic under-estimation of extreme torque, thrust, and thus load changes, which can be comparable to Fig. 1. Most interestingly these load features are not grasped by the characterization based on standard rain flow counting methods. The intermittent statistics of wind and loads are then transferred into an evenly intermittent signal of the electrical power output. With a growing share of wind energy fed into the electrical grid, the high probabilities of extreme changes will have a more and more significant impact on the grid. Another important aspect also becomes clear from these results. Short time fluctuations are not smoothed out by, e.g., some possible spatial averaging or rotational inertia of the rotor. In contrast the nature of the turbulent wind amplifies significantly the effects of the short time fluctuations. For further developed WECs of the future, e.g., the 10 MW



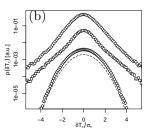


Figure 12: PDFs of (a) rotor torque increments, $\delta Q_{\tau} = Q(t+\tau) - Q(t)$, and (b) rotor thrust increments, $\delta T_{\tau} = T(t+\tau) - T(t)$, derived from simulations of the WInd-PACT 1.5 MW virtual turbine. Wind inflow data were used from the GROWIAN wind field measurement (circles, top), as generated by a stochastic intermittent wind field model (squares, middle), and from the output of the TurbSim software using the Kaimal model (diamonds, bottom). Gaussian PDFs are shown as dashed lines for comparison. Time scale τ is 1s for all presented PDFs. Results of (a) have been published in [31].

class, these turbulent properties have to be considered even more seriously.

To conclude, with the statistics of rotor torque and thrust increments we achieve a complete characterization of the forces at the rotor of WECs. We find that the intermittency of the wind is transferred to the generator by the torque, as well as to the complete structure of the WEC by the thrust forces. The resulting electrical power output of these intermittent input forces will be subject of the following section.

3 Characterisation and modeling of wind-generated electrical power

Throughout the previous sections, it could be demonstrated that the intermittent nature of atmospheric turbulence influences all stages of the wind energy conversion process. The wind imposes its intermittent character upon all relevant quantities, such as wind speeds, mechanical forces and torques, and electrical power output of WEC. The highly dynamical character of the power conversion process and the intermittent properties of the electrical power output have been shown before [33, 34, 32]. They are confirmed by the results of this section, cf. Fig. 15(b).

Future sustainable energy supply systems will have to manage large shares of fluctuating energy sources such as wind energy. This constitutes a demand of properly modeling the high frequency dynamics of these energy conversion systems, including their nonlinear and intermittent properties. As an alternative to highly detailed, complex (and thus computationally expensive) models the usage of stochastic models has recently found a wide range of applications [35, 36]. Generally spoken, for complex systems this approach tries to separate only few crucial variables from a larger number of less important ones, which are then replaced by simple noise terms. By doing so, in many cases

¹so-called order parameters, following [37]

simply structured models are obtained which nevertheless cover the essential dynamics of the system under investigation. Their parameters can be derived directly from measurement data, cf. [36].

Recently the Langevin Power Curve (LPC) has been developed as a dynamical power characteristic of WECs [33, 34, 38]. By this method, for each wind speed the stable (or attractive) fixed points of the energy conversion dynamics are obtained. Together they constitute the LPC of the WEC, which provides important information, complementary to the current industry standard IEC 61400-12-1 [2].

Here we extend this concept and propose a stochastic model of the electrical power output of WEC, driven by the inflowing wind. The structure of the model aims towards the high-frequency dynamics of the conversion from wind speed to electrical power. The power output P(t) is modeled by a stochastic differential equation, namely the Langevin equation [39]

$$\frac{d}{dt}P(t) = D^{(1)}(P;u) + \sqrt{D^{(2)}(P;u)} \cdot \Gamma(t).$$
 (4)

Here $D^{(1)}(P;u)$ and $D^{(2)}(P;u)$ are the drift and diffusion matrices, respectively, and $\Gamma(t)$ is a Gaussian white noise with mean value $\langle \Gamma(t) \rangle = 0$ and variance $\langle \Gamma^2(t) \rangle = 2$. The drift and diffusion matrices $D^{(1)}(P;u)$ and $D^{(2)}(P;u)$ can be estimated directly from measurement data (sampled at the order of 1Hz), as follows [39, 33]

$$D^{(n)}(P;u) = \frac{1}{n!} \lim_{\tau \to 0} \frac{1}{\tau} \left\langle \left[P(t+\tau) - P(t) \right]^n \middle| P(t) = P; u(t) = 0 \right\rangle$$
(5)

where $\langle \cdot | \cdot \rangle$ denotes conditional ensemble averaging. Note that u(t) is thus conditioned on a fixed value u. An illustration of $D^{(1)}$ is given in Fig. 13(a). The drift field (or matrix) $D^{(1)}$ represents the dynamical map of the conversion process $u(t) \to P(t)$. The power production is attracted towards the stable fixed points P(u), while the turbulent wind fluctuations continuously drive the system away. This corresponds to the structure of the Langevin equation (4), where the drift field $D^{(1)}$ represents the attractor displayed in Fig. 13(a), and where the diffusion field $D^{(2)}$ quantifies additional, random fluctuations stemming from turbulence. A second example of a drift field is presented in Fig. 13(b). Here the dynamics of the torque depending on the rotational speed is displayed, showing that the method of the LPC is not limited to the dynamics of power output. It rather defines a general mathematical tool for analyzing the dynamics of complex, noisy, and noise-driven systems.

While only the drift field with its fixed points as shown in Fig. 13 defines the LPC, the Langevin equation Eq. (4) uses both the drift and diffusion matrices. Once these have been estimated from a dataset, they can be used in the Langevin equation to simulate the power output P(t) for any given wind speed u(t).

As a first hint for the validity of the stochastic model², a

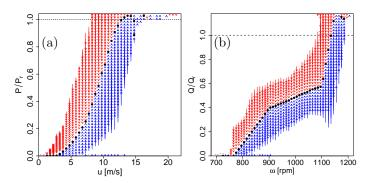


Figure 13: Drift fields $D^{(1)}$ derived from WEC measurements, represented qualitatively using arrows. The local value of the drift $D^{(1)}$ is represented by the direction and length of each arrow, while the color also indicates the direction of the drift. The black dots represent the stable fixed points where $D^{(1)} = 0$. (a) Drift field $D^{(1)}(P; u)$ of electrical power output vs. wind speed. Here the black dots repesent the Langevin Power Curve [40]. (b) Drift field $D^{(1)}(Q;\omega)$ of rotor torque vs. angular velocity. For this analysis the torque was obtained from available measurements of angular velocity and electrical power output. Power and torque are normalized by their rated values P_r and Q_r , respectively.

visual comparison of P and P^* is given in Fig. 14. A statistical comparison is performed based on power spectral densities in Fig. 15(a). The overall shape of the spectrum is repro- $D^{(n)}(P;u) = \frac{1}{n!} \lim_{\tau \to 0} \frac{1}{\tau} \left\langle [P(t+\tau) - P(t)]^n | P(t) = P; u(t) = u \right\rangle$ ties in Fig. 15(a). The overall shape of the spectrum is reproduced by the stochastic model. The most striking deviation is observed at frequency $f \approx 1 \,\mathrm{Hz}$, which corresponds to a 1 Hz oscillation in the measured time series P(t). We believe this is due to the interaction of the tower with the rotating blades of the WEC³, which happens in the same frequency range. As our model is based on a first-order stochastic differential equation Eq. (4) it can in principle not reproduce a single-frequency oscillation like this. As a future improvement, a suitable oscillation could be added to the model to compensate for this limitation.⁴ Figure 15(b) illustrates the ability of the model to reproduce the intermittency of the original power signal. For example, changes in power production up to $\pm 100 \,\mathrm{kW}$ within $0.8 \,\mathrm{s}$ occur. This aspect is especially important on shorter time scales when fast wind gusts are converted into fast power gusts. Moderate deviations are observed on the shorter time scales, where the model behaves less intermittent than desired. Overall, the stochastic model obtains valuable results as spectral properties and intermittency are mostly well reproduced. Its fast and flexible structure makes the stochastic method useful for a realistic modeling of single WECs, wind farms and wind farm clusters (as will be shown elsewhere).

> It should nevertheless be noted that the purpose of this model is not to compete with current full-featured multibody models of WECs, such as FAST [25] or FLEX [42]. In

 $^{^2{\}rm The}$ results of the stochastic model are presented here for a dataset obtained from a numerical model, see details in Ref. [41]. Similar results were obtained for various measurement datasets, for which the results were surprisingly good, even though the noise by the turbulent inflow will not fulfill the conditions of a Langevin noise.

³It should be noted that not only the tower interaction can generate periodic fluctuations in the order of 1 Hz. Additional contributions from the rotating rotor are not identified here.

⁴Here it should be noted also that in a typical measurement setup with 1 Hz sampling frequency this oscillation would not be visible, making the validation of such a model extension impossible in most cases.

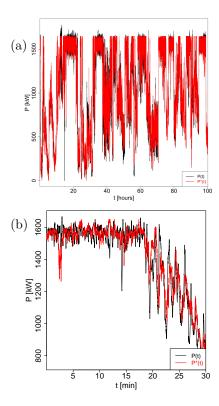


Figure 14: Comparison of P(t) (black) and $P^*(t)$ (red) for (a) 100 h and (b) 30 min at sampling frequency 2.5 Hz.

contrast to these, the proposed model is highly simplified and does not aim at a detailed model of the processes inside a WEC. It rather constitutes an effective model of a WEC as a whole, considering only the wind as input and a single output quantity, such as electrical power or torque. While the descriptive power of our model in this sense is limited, it benefits from high numerical efficieny as well as easy and straightforward parameter retrieval.

We can conclude that the stochastic model is able to capture consistently the dynamics of power or torque, depending on wind speed or rotational frequency, respectively. Once the parameters have been estimated from measurements, for simulations only wind speed time series are required as input. In the results especially the typical intermittency is reproduced.

4 Outlook: n-point statistics and forecasting

Up to this point our analysis, modeling, and experiments concerning atmospheric turbulence were concentrating on increments of relevant signals, e.g., wind speeds, torque, and electrical power. These increment statistics can be obtained in a straightforward way and it has been demonstrated that they are of high relevance.

Based on recent results presented in Sec. 2.1 we are presently working on the decomposition of atmospheric turbulence into components which behave similar to homogeneous isotropic turbulence. For this case, in the recent years

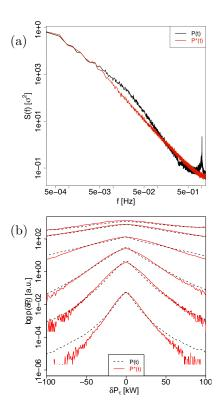


Figure 15: (a) Power spectral density S(f) of P (black) and P^* (red). S(f) is normalized by the variance σ^2 of the time series. (b) PDF of power increments δP_{τ} for various scales $\tau = (0.4, 0.8, 1.6, 6.4, 25.6, 26214.4)$ s from bottom to top, curves are shifted vertically for clarity. The solid red lines are estimated from P^* and the black dashed lines from P. The vertical axis is represented using a logarithmic scale.

a framework of stochastic analysis and characterization has been developed, which grasps the complete statistical properties of turbulence in terms of arbitrary n-scale joint probabilities [43, 44, 35, 36]. Moreover, a method has been presented for the multiscale reconstruction of real turbulent time series [45, 46].

From the combination of these work topics in the future we hope to make adcvances towards a multipoint description framework for atmospheric turbulence. This would mean also a proper characterization of multiscale joint probabilities, which correspond to coherent structures in wind fields. As a consequence, also multiscale short-time forecasting of wind events, such as gusts and clustering effects, could be possible with only little computational effort, compare Ref. [45].

5 Conclusions

In this contribution, fundamental as well as applied aspects have been presented for advanced statistics, modeling and experiments concerning atmospheric turbulence. Based on the fact that atmospheric turbulence exhibits complex statistical properties especially in wind speed increment and fluctuation PDFs, we proposed an advanced characterization. Similar to the modeling and characterization of wind

data in [5], here we achieve a proper description and modeling of atmospheric fluctuation PDFs. First successful attempts have been made towards the decomposition of atmospheric turbulence into subsets which share the properties of homogeneous isotropic turbulence. An outlook to even more elaborate modeling and characterizations has been given. Based on these results a more realistic, yet still practicable, characterization of atmospheric wind becomes possible, overcoming the implicit assumption of Gaussianity in current methods and standards.

As turbulence, in principle, has to be considered an open problem of classical physics, experiments form an indispensable component of our work. For the reproduction of crucial properties of atmospheric flows the active grid offers extreme flexibility in the design and control of wind tunnel experiments. Investigations of the reproducibility of flow structures have been presented as well as the application to testing and characterization of anemometer properties.

The impact of atmospheric turbulence on wind energy conversion is investigated in two separate aspects. Numerical modeling of turbines shows evidence that the intermittent nature of the wind leads to high probabilities of extreme load changes in both torque and thrust. These results completely characterize the forces induced by the rotor to the drive train of a WEC. Accordingly intermittent statistics are found in the electrical power output of both numerical models and real turbines, which constitutes the input to the electrical grid. An extended approach can model the power output of a WEC based on wind measurement data, reproducing properly the statistical properties of a real power output signal.

The common assumption of Gaussian wind statistics necessarily neglects these intermittency effects. We propose that more realistic statistical description and modeling of atmospheric turbulence is necessary to advance not only in science but also in engineering as well as in manufacturing and operation of WECs.

Stochastic methods are shown as appropriate tools to characterize the dynamics and intermittency of the wind energy conversion process in more details, and thus provide valuable, additional information to standard methods. The results presented show that these methods have a large potential of application for further aspects of wind energy.

References

- [1] X. Lu, M.B. McElroy, and J. Kiviluoma, *Global potential for wind-generated electricity*, Proceedings of the National Academy of Sciences 106 (2009), pp. 10933–10938.
- [2] IEC, International Standard 61400: Wind Turbines, International Standard 61400-12-1, International Electrotechnical Commission, 2005.
- [3] M. Ragwitz, and H. Kantz, *Indispensable finite time corrections for Fokker-Planck equations from time series data*, Physical Review Letters 87 (2001), p. 254501.

- [4] F. Böttcher, C. Renner, H.P. Waldl, and J. Peinke, On the statistics of wind gusts, Boundary-Layer Meteorology 108 (2003), pp. 163–173.
- [5] F. Böttcher, S. Barth, and J. Peinke, Small and large fluctuations in atmospheric wind speeds, Stochastic Environmental Research and Risk Assessment 21 (2007), pp. 299–308.
- [6] J. Vindel, C. Yague, and J.M. Redondo, Structure function analysis and intermittency in the atmospheric boundary layer, Nonlinear Processes in Geophysics 15 (2008), pp. 915–929.
- [7] L. Liu, F. Hu, X.L. Cheng, and L.L. Song, Probability Density Functions of Velocity Increments in the Atmospheric Boundary Layer, Boundary-Layer Meteorology 134 (2010), pp. 243–255 10.1007/s10546-009-9441-z.
- [8] J.F.m.c. Muzy, R. Baïle, and P. Poggi, Intermittency of surface-layer wind velocity series in the mesoscale range, Phys. Rev. E 81 (2010), p. 056308.
- [9] R.W. Stewart, J.R. Wilson, and R.W. Burling, Some statistical properties of small scale turbulence in an atmospheric boundary layer, Journal of Fluid Mechanics 41 (1970), pp. 141–152.
- [10] H. Tennekes, Intermittency of the small-scale structure of atmospheric turbulence, Boundary-Layer Meteorology 4 (1973), pp. 241–250.
- [11] P. Tavner, Y. Qiu, A. Korogiannos, and Y. Feng, The Correlation Between Wind Turbine Turbulence and Pitch Failure, in Proceedings of EWEA 2011, 2011.
- [12] M. Wächter, A. Rettenmeier, M. Kühn, and J. Peinke, Characterization of short time fluctuations in atmospheric wind speeds by LIDAR measurements, Meteorologische Zeitschrift 18 (2009), pp. 277–280.
- [13] M. Nielsen, G. Larsen, J. Mann, S. Ott, K. Hansen, and B. Pedersen, Wind Simulation for Extreme and Fatigue Loads, Riso-R-1437(EN), Risø DTU, 2003.
- [14] B. Castaing, Y. Gagne, and E.J. Hopfinger, Velocity probability density functions of high Reynolds number turbulence, Physica D 46 (1990), pp. 177–200.
- [15] A. Morales, M. Wächter, and J. Peinke, Characterization of wind turbulence by higher-order statistics, Wind Energy (2011).
- [16] U. Frisch Turbulence: the legacy of A. N. Kolmogorov, Cambridge University Press, 2001.
- [17] K.S. Hansen, and G.C. Larsen, Characterising Turbulence Intensity for Fatigue Load Analysis of Wind Turbines, Wind Engineering 29 (2005), pp. 319–329.
- [18] H. Makita, Realization of a large-scale turbulence field in a small wind tunnel, Fluid Dynamics Research 8 (1991), pp. 53 – 64.

- [19] L. Mydlarski, and Z. Warhaft, On the onset of high-Reynolds-number grid-generated wind tunnel turbulence, Journal of Fluid Mechanics 320 (1996), pp. 331– 368.
- [20] P. Knebel, A. Kittel, and J. Peinke, Atmospheric wind field conditions generated by active grids, Experiments in Fluids (2011), pp. 1–11 10.1007/s00348-011-1056-8.
- [21] A. Wiesner, F. Fiedler, and U. Corsmeier, The Influence of the Sensor Design on Wind Measuremnets with Sonic Anemometer Systems, Journal of Atmospheric and Oceanic Technology 18 (2001), pp. 1585–1608.
- [22] H. Cekli, and W. Watervan de, Tailoring turbulence with an active grid, Experiments in Fluids 49 (2010), pp. 409–416 10.1007/s00348-009-0812-5.
- [23] G.H. Good, and Z. Warhaft, On the probability distribution function of the velocity field and its derivative in multi-scale turbulence, Physics of Fluids 23 (2011), p. 095106.
- [24] H. Günther, and B. Hennemuth Erste Aufbereitung von flächenhaften Windmessdaten in Höhen bis 150 m, Deutscher Wetter Dienst, BMBF-Projekt 0329372A, 1998.
- [25] J. Jonkman, NWTC Design Code FAST, NREL/EL-500-38230, National Renewable Energy Laboratory, Golden, Colorado, USA, 2005.
- [26] D.J. Malcolm, and A.C. Hansen WindPACT turbine rotor design study, National Renewable Energy Laboratory, Golden, Colorado, 2002 NREL/SR-500-32495.
- [27] F. Körber, G. Besel, and H. Reinhold Meßprogramm an der 3MW-Windkraftanlage GROWIAN: Förderkennzeichen 03E-4512-A, Große Windenergieanlage Bau- u. Betriebsgesellschaft, Hamburg, 1988 Bundesministerium für Forschung und Technologie.
- [28] N. Kelley, and B. Jonkman, NWTC Design Codes: TurbSim; http://wind.nrel.gov/designcodes/preprocessors/turbsim/accessed 17.6.2011.
- [29] D. Kleinhans, and R. Friedrich, Simulation of intermittent wind fields: A new approach, in DEWEK 2006 Proceedings, Bremen (Germany), 2006.
- [30] D. Kleinhans, Stochastische Modellierung komplexer Systeme, Universität Münster, 2008.
- [31] T. Mücke, D. Kleinhans, and J. Peinke, Atmospheric turbulence and its influence on the alternating loads on wind turbines, Wind Energy 14 (2011), pp. 301–316.
- [32] J. Gottschall, and J. Peinke, Stochastic modelling of a wind turbine's power output with special respect to turbulent dynamics, Journal of Physics: Conference Series 75 (2007), p. 012045.

- [33] E. Anahua, S. Barth, and J. Peinke, *Markovian power curves for wind turbines*, Wind Energy 11 (2008), pp. 219–232.
- [34] J. Gottschall, and J. Peinke, How to improve the estimation of power curves for wind turbines, Environmental Research Letters 3 (2008), p. 015005 (7pp).
- [35] R. Friedrich, J. Peinke, and M.R.R. Tabar, 2009, Importance of Fluctuations: Complexity in the View of Stochastic Processes. in *Encyclopedia of Complexity and System Science* Springer, Berlin in print.
- [36] R. Friedrich, J. Peinke, M. Sahimi, and M.R.R. Tabar, Approaching Complexity by Stochastic Methods: From Biological Systems to Turbulence, Physics Reports (2011) (accepted).
- [37] H. Haken Advanced synergetics: Instability hierarchies of self-organizing systems and devices, Springer, 1983.
- [38] M. Wächter, P. Milan, T. Mücke, and J. Peinke, Power performance of wind energy converters characterized as stochastic process: applications of the Langevin power curve, Wind Energy (2010) Published online, DOI: 10.1002/we.453.
- [39] H. Risken The Fokker-Planck equation, Springer, Berlin, 1984.
- [40] P. Milan, T. Mücke, A. Morales, M. Wächter, and J. Peinke, Applications of the Langevin Power Curve, in Proceedings of EWEC 2010, Warshaw, 2010.
- [41] P. Milan, M. Wächter, and J. Peinke, Stochastic Modeling of Wind Power Production, in Proceedings of EWEA 2011, Brussels, 2011.
- [42] S. Øye, FLEX 5 User Manual, , Danske Techniske Hogskole, Lyngby, 1999.
- [43] R. Friedrich, and J. Peinke, Description of a Turbulent Cascade by a Fokker-Planck Equation, Physical Review Letters 78 (1997), p. 863.
- [44] C. Renner, J. Peinke, and R. Friedrich, Experimental indications for Markov properties of small-scale turbulence, Journal of Fluid Mechanics 433 (2001), pp. 383– 409.
- [45] A.P. Nawroth, and J. Peinke, Multiscale reconstruction of time series, Physics Letters A 360 (2006), pp. 234– 237.
- [46] R. Stresing, and J. Peinke, Towards a stochastic multipoint description of turbulence, New Journal of Physics 12 (2010), p. 103046.